



OPEN

# Furosemide drug as a corrosion inhibitor for carbon steel in 1.0 M hydrochloric acid

Samir Abd El Maksoud<sup>1</sup>✉, Abd El Aziz Fouda<sup>2</sup> & Haby Badawy<sup>2</sup>

Furosemide (4-chloro-2-furan-2-ylmethylamino-5-sulfamoylbenzoic acid) was examined as an inhibitor for the corrosion of carbon steel (CS) in 1.0 M HCl. The investigation included mass loss (ML) and electrochemical techniques: potentiodynamic polarization (PP), electrochemical impedance spectroscopy (EIS), and electrochemical frequency modulation (EFM). The efficiency of inhibition rises with increasing Furosemide concentration and temperature. This compound follows the Temkin isotherm with good fit. The presence of varying quantities influences both anodic metal dissolution and cathodic hydrogen evolution. Scanning electron microscopy (SEM), atomic force microscopy (AFM), X-ray photoelectron spectroscopy (XPS), and Fourier transform infrared spectroscopy (FT-IR) were used to detect the effect of the compound on the CS surface. The molecular inhibitory effect of Furosemide was demonstrated using quantum chemical calculations, and the molecular simulation results demonstrated the adsorption on the carbon steel surface.

**Keywords** Furosemide, Carbon steel, Potentiodynamic, Impedance, HCl

The study of carbon steel corrosion in acidic destructive solutions is essential in industry<sup>1</sup>. The acidic solution is widely used to: (1) remove scale in industrial operations; (2) treat water plants; and (3) pickle oil recovery and petrochemical processes. Acid aqueous solutions are among the most corrosive media, and CS is extensively used in pipelines, in the oil and gas industries. Inhibitors are used to prevent CS corrosion<sup>2</sup>. The corrosion inhibition efficacy of the compounds is related to the adsorption capabilities, which form an adsorbing layer on CS (physisorption or chemisorption)<sup>3</sup>. The adsorption is influenced by the nature and state of the metal surface, the type of corrosive media, and the chemical structure of the inhibitor<sup>4,5</sup>.

Organic compounds contain heteroatoms such as sulphur, nitrogen, oxygen, and an aromatic ring, were extensively utilized as corrosion inhibitors<sup>6</sup>. Most organic compounds are toxic and harmful to the environment<sup>7–13</sup>. Because of the toxicity of these organic inhibitors, there is an opportunity to investigate the application of environmentally non-toxic inhibitors<sup>14–16</sup>. It is critical to use friendly acid corrosion inhibitors that are low-cost, non-hazardous, and efficient<sup>17–25</sup>. The corrosion inhibition activity of several medications has been studied in order to determine their potential use as a competitive class of green corrosion inhibitors. Many medicines' corrosion inhibition performances have been investigated<sup>26–46</sup>. The current research aims to evaluate Furosemide as a corrosion inhibitor for CS corrosion in 1.0 M HCl. The inhibition of CS corrosion in 1.0 M HCl was determined and confirmed using chemical and electrochemical techniques. The adsorbed film on the metal surface was characterized using AFM, SEM, EDX, FT-IR, and XPS analyses.

## Materials and methods

### Materials

Chemical composition of carbon steel: 0.14% C, 0.52% Mn, 0.05% P, 0.02% Si, 0.03% Cr, 0.02% Ni, 0.002% P, 0.04% S, 0.02% Cu, and the rest Fe. The aggressive solution of 1.0 M HCl was prepared by dilution with bidistilled water. The inhibitor structure is illustrated in Table 1. The stock solution of Furosemide (1000 ppm) concentration was prepared by dissolving the calculated mass in bidistilled water. The concentrations used ranged from 50 to 300 ppm.

<sup>1</sup>Department of Chemistry, Faculty of Science, Port Said University, Port Said, Egypt. <sup>2</sup>Department of Chemistry, Faculty of Science, Mansoura University, Mansoura 35516, Egypt. ✉email: samirabdelhady@yahoo.com

Structure	IUPAC name	Molecular weight	Chemical formula
	4-Chloro-2-(furan-2-ylmethylamino)-5-sulfamoylbenzoic acid	330.74 g/mol	C <sub>12</sub> H <sub>11</sub> ClN <sub>2</sub> O <sub>5</sub> S

**Table 1.** The molecular structures, name, chemical formula and molecular weight of Furosemide.

## Methods

### Mass loss

The test specimens of CS with the dimensions (2 × 2 × 0.1 cm) were used. The samples were abraded with emery sheet grit (sizes 400, 600, 800, and 1200) to ensure the softness of the CS surface and then washed with bidistilled water, degreased with acetone, dried and weighed. The weighted samples were immersed in 100 ml of 1.0 M HCl in the absence and presence of different concentrations of the examined compound. The time of immersion was recorded at various temperatures; the temperature was controlled in the water by the thermostatic bath with an accuracy of ± 0.1 °C. After the immersion time, CS sheets were removed from the solution, washed with bidistilled water, dried, and weighed. Experiments were repeated three times with diverse samples to confirm the repeatability of the results.

The IE% and surface coverage ( $\theta$ ) of the inhibitor were calculated by Eq. (1)

$$\text{IE\%} = \left( 1 - \left[ \frac{W}{W_0} \right] \right) \times 100 = \theta \times 100 \quad (1)$$

where  $W_0$  and  $W$  values are the mass loss without and with different concentrations of the inhibitor, respectively.

### Electrochemical techniques

Potentiodynamic polarization, electrochemical impedance spectroscopy, and the electrochemical frequency modulation technique were utilized to detect the corrosion behaviour of CS in 1.0 M HCl. All the experiments were carried out in glass cells with three electrodes. The counter electrode was a Pt electrode, the reference electrode was a saturated calomel electrode, and the working electrode was CS. The working electrode area was 1.0 × 1.0 cm. It was rinsed, polished with emery paper of different grades, washed and degreased with acetone, then washed with bidistilled water. All the experiments were carried out at 25 ± 1 °C. The open-circuit potential was started for 30 min and then recorded until the steady state of the specimens was reached. All the electrochemical experiments were carried out using a potentiostat/galvanostat from Gamry Instrument Series G 750.

**Potentiodynamic technique (PP).** In this method, the potential was applied from − 0.750 to − 0.250 V at a scan rate of 1 mV s<sup>−1</sup>, and the corrosion current density ( $i_{\text{corr}}$ ) was estimated. The IE% and  $\theta$  can be calculated from Eq. (2)

$$\text{IE\%} = \left( 1 - \left[ \frac{i_{\text{corr}}(\text{inh.})}{i_{\text{corr}}(\text{free})} \right] \right) \times 100 = \theta \times 100 \quad (2)$$

$i_{\text{corr}}^0$  and  $i_{\text{corr}}$  are the current densities without and with inhibitors, respectively.

**Electrochemical impedance spectroscopy (EIS).** Impedance measurements were performed in the frequency range from 100 kHz to 0.1 Hz using 5 mV amplitude. IE% and  $\theta$  were estimated from Eq. (3)

$$\text{IE\%} = \left( \frac{R_p^0 - R_p}{R_p^0} \right) \times 100 = \theta \times 100 \quad (3)$$

$R_p^0$  and  $R_p$  are the polarization resistances with and without inhibitors, respectively. The double-layer capacitance ( $C_{\text{dl}}$ ) values in the presence of different concentrations were determined from Eq. (4):

$$C_{\text{dl}} = \frac{1}{2\pi f_{\text{max}} R_{\text{ct}}} \quad (4)$$

where  $f_{\text{max}}$  is the value of maximum frequency.

**Electrochemical frequency modulation technique (EFM).** EFM can be used as a fast and non-destructive method for CS corrosion without knowledge of the Tafel slope. EFM technique with amplitudes of 10 mV and two sine waves of 2 and 5 Hz High peaks are used to calculate the current density ( $i_{\text{corr}}$ ), Tafel slope ( $\beta_c$  and  $\beta_a$ ) and the causality factors (CF-2 and CF-3).

### Surface investigations

**Scanning electron microscopy.** After dipping the CS specimen in 1 M HCl without and with 300 ppm Furosemide for a day at 25 °C, the surface of the CS specimen was investigated. A scanning electron microscope (SEM; JEOL JSM-5500, Japan) was used. SEM images of the metal surface were taken at a magnification of 2000.

**Atomic force microscopy (AFM).** The outer surface roughness can be assessed using an AFM instrument that creates a topographic surface map with a distinct resolution. Surface roughness results from variations in a surface's ideal shape induced by corrosion or inhibitor adsorption. Thermo Fisher Nicolet IS10 (scanning probe microscope) was employed.

**X-ray photoelectron spectroscopy (XPS).** These studies were carried out using a highly efficient system that uses XPS to identify the binding energies of various bonds discovered on the carbon steel surface, allowing the adsorbed atoms and functional groups on the metal surface to be determined. K-ALPHA (Thermo Fisher Scientific, USA) was used.

**Fourier-transform infrared spectroscopy (FTIR).** FTIR spectra of pure solutions of the inhibitor and carbon steel sheets immersed in 1 M HCl plus the optimal concentration of the inhibitor for 24 h were measured using a PerkinElmer 1600 spectrophotometer.

### Simulation analysis

The quantum chemical parameters were found by MSD Mol440<sup>47</sup>, which use efficient density theory (DFT). The chemical quantum parameters, the highest occupied molecular orbital ( $E_{\text{HOMO}}$ ) and the lowest unoccupied molecular orbital ( $E_{\text{LUMO}}$ ), dipole moments ( $\mu$ ), energy gapping ( $\Delta E$ ), hardness ( $\eta$ ), softness ( $\sigma$ ), ionization potentials (I), and electronegativity (X) were calculated for the inhibitor.

## Results and discussion

### Mass loss (ML) method

#### Effect of inhibitor concentrations

Figure 1 represents the relation between mass loss and time for CS in the absence and presence of various concentrations of Furosemide in 1.0 M HCl at 25 °C. The data derived from the mass loss method are presented in Table 2. The data revealed that the mass loss and the corrosion rate decreased with increasing concentrations. The increase in the IE% was due to the barrier formation of inhibitors on the metal surface, which decreases the dissolution of the metal<sup>48</sup>. IE% for CS corrosion was evaluated from Eq. (1).

#### Effect of temperature

The ML method was used to study the effect of temperature on the corrosion rate of CS in 1.0 M HCl containing different concentrations. Figure 2 represents the effect of temperature on the IE% at different concentrations of the studied compound on CS dissolution in a 1.0 M HCl solution. The results obtained are illustrated in Table 3. From the results, we can conclude that the corrosion rate increases in the corrosive medium with increasing temperature. The inhibition efficiency increased with increasing solution temperature, which indicates the chemical absorption type of the inhibitor on the CS surface<sup>49</sup>.

#### Activation thermodynamic parameters

The corrosion rate of the reaction is influenced by the temperature; Eq. (5) specifies this relation according to Arrhenius<sup>50,51</sup>:

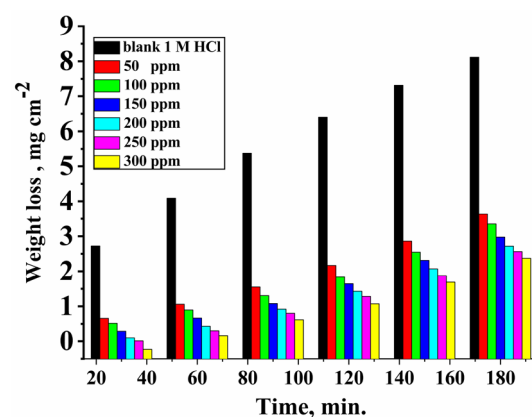


**Figure 1.** Weight loss vs. time for the corrosion of CS in 1.0 M HCl without and with various concentrations from Furosemide at 298 K.

Conc. (ppm)	Temp. (K)	ML (mg cm <sup>-2</sup> )	k <sub>corr</sub> × 10 <sup>3</sup> (mg cm <sup>-2</sup> min <sup>-1</sup> )	θ	IE %
Blank	298	6.4	53.33	–	–
50		1.87	15.64	0.706	70.6
100		1.65	13.82	0.740	74.0
150		1.46	12.21	0.771	77.1
200		1.32	11.02	0.793	79.3
250		1.17	9.78	0.816	81.6
300		1.07	8.93	0.832	83.2

**Table 2.** Mass loss data for CS corrosion at 120 min in 1.0 M HCl without and with various concentrations from Furosemide at 298 K.

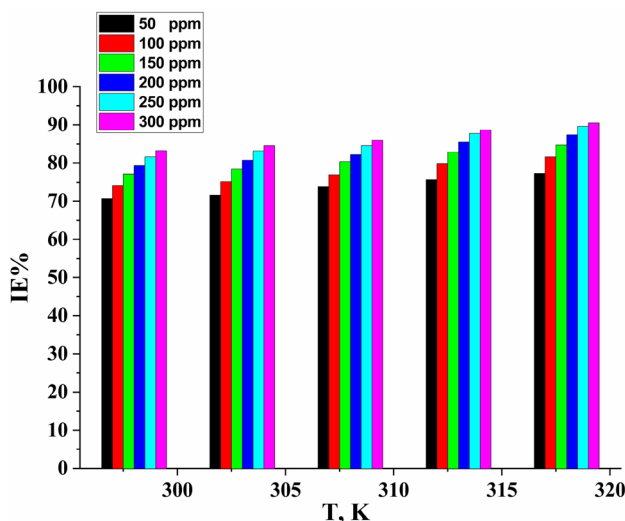


**Figure 2.** Effect of temperature on the IE% at various concentrations from Furosemide for CS in 1.0 M HCl solution at different temperatures.

$$k_{\text{corr}} = A \exp(E_a^*/RT) \quad (5)$$

where A is the Arrhenius constant,  $E_a^*$  is the activation energy, T is the absolute temperature and R is the gas constant.

Figure 3 shows the plot of  $\log k_{\text{corr}}$  vs.  $1/T$  with straight lines; from the line's slopes, we can calculate  $E_a^*$ . The values of  $E_a^*$  are calculated and reported in Table 4.

From the transition state theory as shown in Eq. (6):

$$k_{\text{corr}} = RT/Nh \exp \Delta S^* \exp^{-\Delta H^*/RT} \quad (6)$$

where  $\Delta S^*$  and  $\Delta H^*$  are the entropy and enthalpy of activation, respectively. Figure 4 shows the Plot of  $\log k_{\text{corr}}/T$  vs.  $1/T$ , giving straight lines from their slopes  $\Delta H^*$  can be calculated and reported in Table 4. The results indicate that  $E_a^*$  values decrease in the presence of an inhibitor compared to their absence, indicating chemical adsorption. The positive values of  $\Delta H^*$  indicate the endothermic activation process, which confirms the chemical adsorption of the investigated inhibitor on the CS surface<sup>52</sup>.

#### Adsorption isotherms

The type and charge of the metal, the structure of the inhibitor, and the composition of the electrolyte all influence inhibitor adsorption on the metal surface<sup>53</sup>. The Temkin isotherm, as illustrated in Eq. (7), well matches the data:

$$q = (2.303/a) \log K_{\text{ads}} + (2.303/a) \log C \quad (7)$$

"a" is the CS's heterogeneous factor (a particle interaction factor), and C is the inhibitor concentration. Plotting  $\theta$  vs.  $\log C$  for inhibitors at different temperatures in Fig. 5 results in straight lines with  $\log K_{\text{ads}}$  slopes and intercepts  $(2.303/a)$ .

The free energy of adsorption ( $G_{\text{ads}}^0$ ) was calculated using  $K_{\text{ads}}$  in Eq. (8) as follows:

Conc. (ppm)	Temp. (K)	ML (mg cm <sup>-2</sup> )	k <sub>corr</sub> × 10 <sup>3</sup> (mg cm <sup>-2</sup> min <sup>-1</sup> )	θ	IE %
Blank	303	7.01	58.42	–	–
50		1.98	16.57	0.716	71.6
100		1.73	14.49	0.751	75.1
150		1.51	12.59	0.784	78.4
200		1.34	11.24	0.807	80.7
250		1.17	9.80	0.832	83.2
300		1.07	8.99	0.846	84.6
Blank B		308	9.62	80.1	–
50	2.52		21.0	0.738	73.8
100	2.21		18.49	0.769	76.9
150	1.88		15.72	0.803	80.3
200	1.71		14.25	0.822	82.2
250	1.48		12.34	0.846	84.6
300	1.35		11.25	0.859	85.9
Blank	313		12.82	106.8	–
50		3.11	25.96	0.756	75.6
100		2.58	21.55	0.798	79.8
150		2.18	18.24	0.829	82.9
200		1.85	15.46	0.855	85.5
250		1.57	13.10	0.877	87.7
300		1.45	12.08	0.886	88.6
Blank		318	15.42	128.5	–
50	3.59		29.95	0.772	77.2
100	2.90		24.18	0.816	81.6
150	2.41		20.09	0.847	84.7
200	1.99		16.63	0.873	87.3
250	1.64		13.68	0.896	89.6
300	1.50		12.50	0.905	90.5

**Table 3.** Mass loss data for CS corrosion at 120 min in 1.0 M HCl without and with various concentrations from Furoseamide at various temperatures 303–318 K.

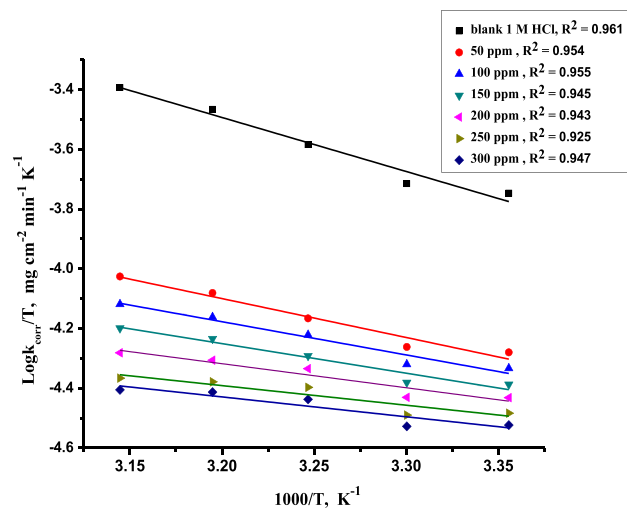


**Figure 3.** Arrhenius plots for dissolution of CS in 1.0 M HCl solution with and without different concentrations of Furoseamide at different temperatures (298–318 K).

Conc. (ppm)	$E_a^*$ (kJ mol <sup>-1</sup> )	$\Delta H^*$ (Kj mol <sup>-1</sup> )	$-\Delta S^*$ (J mol <sup>-1</sup> K <sup>-1</sup> )
0.0	37.2	34.6	153.6
50	24.5	21.9	201.8
100	19.2	16.7	219.9
150	17.3	14.7	227.4
200	15.4	12.8	234.4
250	13.8	11.2	240.2
300	13.1	10.5	243.1

**Table 4.** Activation thermodynamic data for dissolution of (CS) in 1.0 M HCl in the absence and presence of various doses of Furosemide at different temperatures (298–318 K).

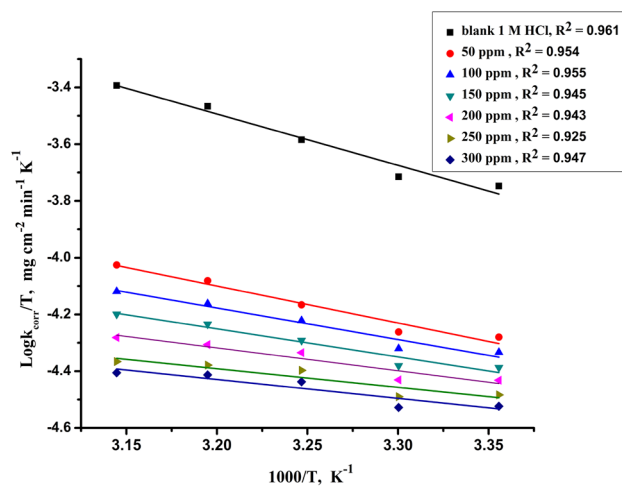


**Figure 4.** Plotting the transition state of  $\text{Log}(k_{\text{corr}}/T)$  vs.  $(1/T)$  for dissolution of CS in 1.0 M HCl solution in the absence and presence of various doses of Furosemide compound at various temperatures (298–318 K).

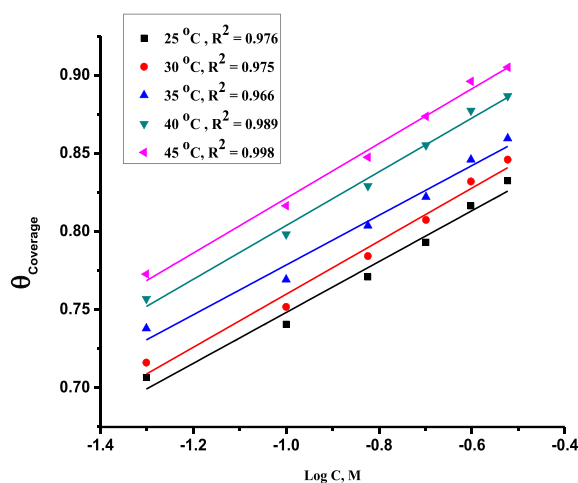


**Figure 5.** Plots of  $\theta$  vs.  $\text{Log } C$  for the Furosemide compound on CS surface in 1.0 M HCl at various temperatures (298–318 K).

The Temkin adsorption isotherm was very good, with a correlation factor  $R^2$  close to 0.978–0.996. The values of “ $a$ ”,  $K_{\text{ads}}$  and  $\Delta G_{\text{ads}}^{\circ}$  were listed in Table 5.  $K_{\text{ads}}$  in Eq. (8) was used to determine the free energy of adsorption ( $\Delta G_{\text{ads}}^{\circ}$ ) as follows:

Temp. (K)	Log ( $K_{\text{ads}}$ M <sup>-1</sup> )	A	$-\Delta G_{\text{ads}}^{\circ}$ (kJ mol <sup>-1</sup> )	$\Delta H_{\text{ads}}^{\circ}$ (kJ mol <sup>-1</sup> )	$-\Delta S_{\text{ads}}^{\circ}$ (J mol K <sup>-1</sup> )
298	5.594	14.0	41.8	77.6	397.9
303	5.708	14.2	43.2		398.8
308	5.909	14.5	45.1		398.4
313	6.168	14.7	47.4		399.4
318	6.439	15.0	49.8		400.7

**Table 5.** Adsorption parameters of Temkin isotherm for the (CS) surface in 1.0 M HCl for Furosemide compound at (298–318 K).

$$\Delta G_{\text{ads}}^{\circ} = -RT \ln (55.5 K_{\text{ads}}) \quad (8)$$

where 55.5 is the molar dosage of H<sub>2</sub>O in the bulk of the solution (mol L<sup>-1</sup>). The calculated data showed that these studied compounds were adsorbed on CS through the lone pair of electrons of heteroatoms (S, N, or O atoms). The  $\Delta G_{\text{ads}}^{\circ}$  and  $K_{\text{ads}}$  values increase with temperature in the range of 298–318 K, also indicating the chemical adsorption of this inhibitor on the CS surface.

Figure 6 as well as Eq. (9), can detect the heat adsorption ( $\Delta H_{\text{ads}}^{\circ}$ )<sup>54</sup>.

$$\text{Log } K_{\text{ads}} = -\Delta H_{\text{ads}}^{\circ}/2.303RT \quad (9)$$

where ( $-\Delta H_{\text{ads}}^{\circ}/2.303R$ ) is the slope of the straight-line Log  $K_{\text{ads}}$  vs.  $1/T$ ,  $\Delta S_{\text{ads}}^{\circ}$  obtained by Eq. (10):

$$\Delta G_{\text{ads}}^{\circ} = \Delta H_{\text{ads}}^{\circ} - T\Delta S_{\text{ads}}^{\circ} \quad (10)$$

Data in Table 5 indicated that  $\Delta G_{\text{ads}}^{\circ}$  values were greater and around  $-40$  kJ mol<sup>-1</sup> dependent on adsorbing by inhibitors on CS surface chemisorption, the coordination of electrons of active groups of the inhibitor molecules to unfilled d-orbitals of CS<sup>55</sup>. The negative values of the free energy of adsorption ( $\Delta G_{\text{ads}}^{\circ}$ ) express the spontaneity of the adsorption. The values of  $\Delta H_{\text{ads}}^{\circ}$  in the present study are higher than  $40$  kJ mol<sup>-1</sup>, which means the chemisorption process<sup>56</sup>. The unshared electron pairs (S, N, and O atoms) might depend on the metal surface of CS. The "a" +ve values are due to the interaction of the adsorbed layers on the CS surface. Furthermore, the values of  $K_{\text{ads}}$  reveal that the increase in the adsorption equilibrium caused by an increase in temperature (Table 5). Entropy values were negative, revealing that the adsorption of the inhibitor was associated with adsorption rather than desorption on the metal surface. Table 5 shows the increase in  $\Delta S_{\text{ads}}^{\circ}$  values as the disorders increase owing to the adsorption of H<sub>2</sub>O molecules by the adsorption of inhibitors on the surface of CS<sup>57</sup>.

## Electrochemical techniques

### Open circuit potential ( $E_{\text{OCP}}$ )

Figure 7 depicts the change in  $E_{\text{OCP}}$  over time obtained for C-steel in 1 M HCl in the absence and presence of various doses of Furosemide at 298 k. The figure demonstrates that  $E_{\text{OCP}}$  in the blank started at  $-573$  mV and then shifted anodically until the steady state was achieved. In the presence of Furosemide,  $E_{\text{OCP}}$  began with a significantly positive potential compared to its absence and later shifted anodically. The shift in  $E_{\text{OCP}}$  becomes more positive as the concentration increases. The highest shift in the value of OCP was 35 mV in the presence of the inhibitor. This behaviour indicates that the corrosion inhibitor functions as a mixed type corrosion inhibitor for C-steel in aggressive 1 M HCl<sup>58,59</sup>.

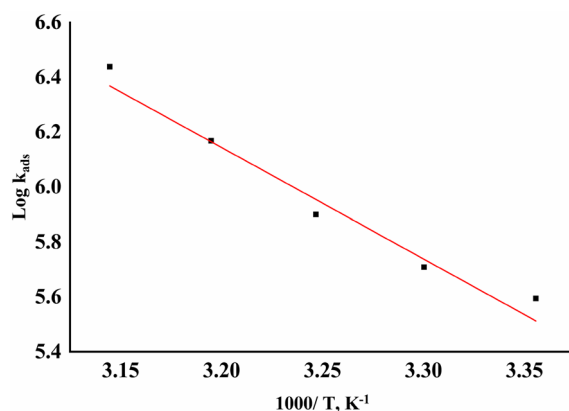


**Figure 6.** Plots of variation of Log  $K_{\text{ads}}$  vs.  $1/T$  for the adsorption of various doses of Furosemide compound on the CS surface in 1.0 M HCl at (298–318 K).

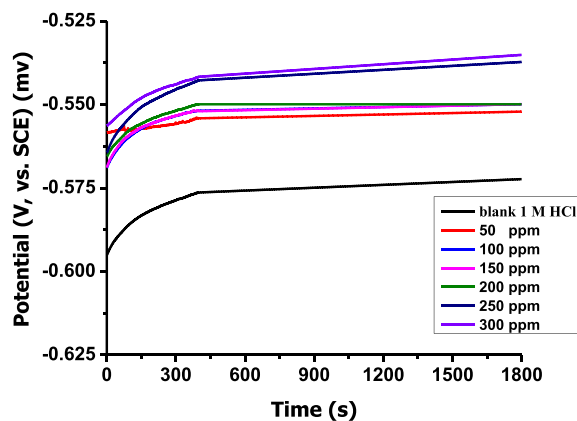


**Figure 7.** Potential-time curves for CS immersed in 1.0 N HCl solution at 298 K without and with different concentrations from Furosemide.

*Potentiodynamic polarization (PP)*

Figure 8 shows the polarization performance of the CS in 1.0 M HCl with and without different doses of the inhibitor. The measured data: corrosion current density ( $i_{corr}$ ), corrosion potential ( $E_{corr}$ ), cathodic Tafel slope ( $\beta_c$ ), Tafel slope ( $\beta_a$ ), ( $\theta$ ), and (IE%) were estimated and reported in Table 6. Moreover, by adding an inhibitor, the corrosion current decreased, indicating that this inhibitor agreed with the suitable inhibitor’s behaviour. The slight change in both Tafel slopes and  $E_{corr}$  indicates that this investigated inhibitor behaves as a mixed type inhibitor<sup>60</sup>. The Tafel lines were parallel with and without inhibitor, indicating that there is no change in the mechanism.

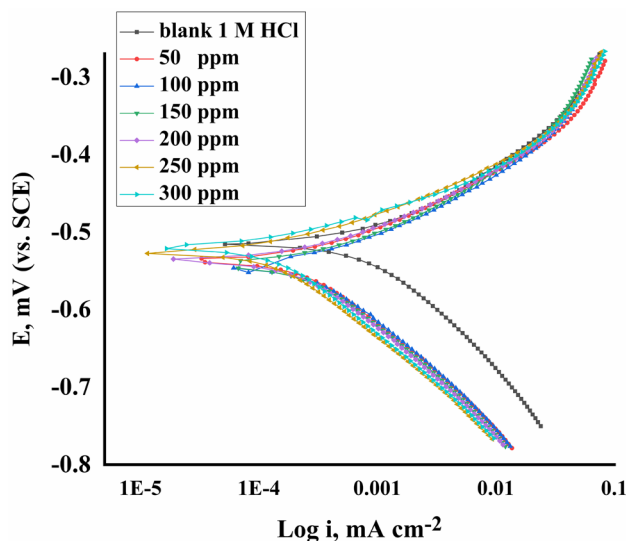


**Figure 8.** Plotting of PP for dissolution of (CS) in 1.0 M HCl using different doses of Furosemide at 298 K.

Conc. (ppm)	$-E_{corr}$ (mV vs. SCE)	$i_{corr}$ ( $\mu\text{A cm}^{-2}$ )	$-\beta_c$ ( $\text{mV dec}^{-1}$ )	$\beta_a$ ( $\text{mV dec}^{-1}$ )	$k_{corr}$ (mpy)	$\theta$	IE %
0	533	1480	210	134	755	–	–
50	522	529	193	108	269.5	0.642	64.2
100	518	480	175	104	245	0.675	67.5
150	520	468	179	106	239	0.683	68.3
200	515	326	190	113	168	0.779	77.9
250	521	212	166	81	111	0.856	85.6
300	520	183	188	76	96	0.876	87.6

**Table 6.** Data of PP of CS in 1.0 M HCl without and with various doses of Furosemide at 298 K.



### Electrochemical impedance spectroscopy

Electrochemical impedance spectroscopy (EIS) is a technique used to gain insight into the characteristics of electrochemical processes that occur on the steel surface in acid solution. Figure 9a shows Nyquist plots of carbon steel with and without various amounts of Furosemide in 1.0 M HCl. They are semicircles moving along the real impedance of the x-axis. However, the smoothness of these semicircles deviated slightly from the classic EIS idea. Metal surface heterogeneity and frequency dispersion can also create imperfect capacitance loops<sup>61</sup>. The semicircle radii are changed by the inhibitor concentrations. The radius of the semicircular lines increases in direct proportion to the concentration. The widths of the capacitance loops are greater in the presence of Furosemide than in its absence, demonstrating that inhibitor molecules can greatly promote steel surface anticorrosion<sup>62</sup>. The concentration of inhibitor molecules adsorbing on carbon steel's surface is proportional to its concentration. The double-layer capacitance ( $C_{dl}$ ) from Eq. (11) can be reproduced using CPE<sup>63</sup>:

$$C_{dl} = Y_o(\omega_{max})n - 1 \quad (11)$$

where  $\omega_{max}$  represents the frequency corresponding to the maximum value of the imaginary component of the Nyquist plot.

Figure 9b shows the correlated equivalent circuit used to model the CS/HCl interface, where  $R_s$  represents the uncompensated solution resistance, the  $R_p$  includes charge transfer resistance ( $R_{ct}$ ), diffuse layer resistance ( $R_d$ ), the accumulated species at the CS/HCl interface ( $R_a$ ), and the resistance of the inhibitor film at the surface<sup>64–67</sup>.

Table 7 shows that  $R_p$  values increase as inhibitor concentration increases. The  $R_p$  value varies between 44.1 and 176.9  $\Omega/\text{cm}^2$ . This could imply that the inhibitor develops a protective coating on the electrode surface at all concentrations. This could imply that the inhibitor develops a protective coating on the electrode surface at

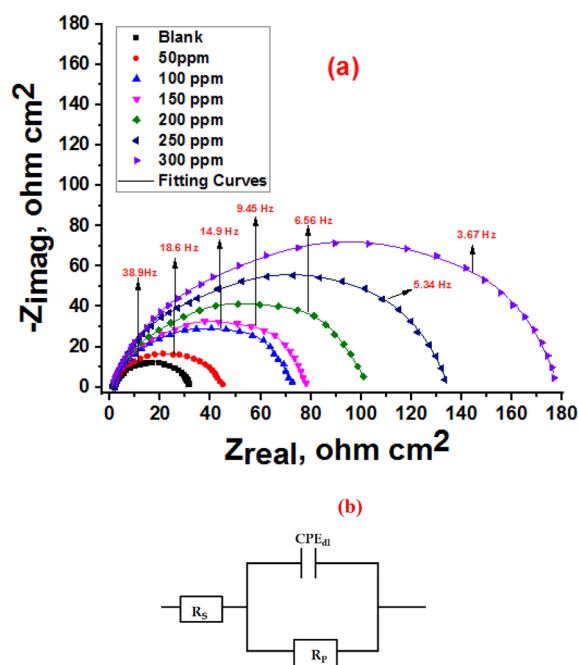


**Figure 9.** (a) EIS spectra of Nyquist for dissolution of CS in 1.0 M HCl without and with various doses of the Furosemide compound at 298 K. (b) Electrochemical equivalent circuit used by fitting the EIS data.

Conc., (ppm)	$R_s$ $\Omega \text{ cm}^2$	$Y_o$ ( $\mu\Omega^{-1} \text{ s}^n \text{ cm}^{-2}$ )	$n$	$R_p$ ( $\Omega \text{ cm}^2$ )	$C_{dl}$ ( $\mu\text{F cm}^{-2}$ )	$\theta$	IE %	Goodness of fit ( $\chi^2$ )
0	1.9	325.6	0.970	30.9	284.4	–	–	$8.24 \times 10^{-3}$
50	1.82	221.7	0.852	44.1	82.9	0.314	29.9	$9.57 \times 10^{-3}$
100	1.64	201	0.811	75.6	75.5	0.605	60.5	$7.44 \times 10^{-3}$
150	1.39	197	0.808	79.4	73	0.628	61.1	$6.54 \times 10^{-3}$
200	1.5	168.5	0.792	102.4	65.4	0.712	69.8	$9.44 \times 10^{-3}$
250	1.88	174	0.782	135.3	60.7	0.781	77.2	$8.78 \times 10^{-3}$
300	1.17	161	0.752	176.2	49.6	0.834	82.5	$6.87 \times 10^{-3}$

**Table 7.** EIS data for the corrosion of (CS) in 1.0 M HCl without and with various doses of Furosemide at 298 K.

all concentrations<sup>68</sup>. As a result, corrosive ions are successfully kept from coming into contact with the working electrode. At the same time, the addition of inhibitors lowers  $C_{dl}$  values by forming a protective layer on the steel surface. The inhibitor exhibits the highest inhibitory efficiency at a concentration of 300 ppm, according to the EIS method. The varying  $n$  values in the presence of inhibitors indicate that the heterogeneous properties of the steel surface have changed. This could be related to the adsorption of inhibitor molecules on the electrode surface<sup>69</sup>.

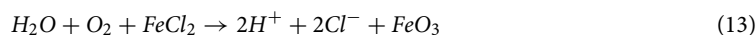
#### Electrochemical frequency modulation

Two sine waves with frequencies of 2 and 5 Hz are supplied to the cell for EFM measurements in the absence and presence of varying doses of the examined substance. The Tafel constants are not required because the results are generated instantaneously with this approach<sup>70</sup>. The output current fluctuates with frequency and is nonlinear. The causality factors (CF-2 and CF-3) acquired from EFM testing are critical because they validate the EFM measurements if their values are near the theoretical values (2 and 3). Harmonic peaks in the output spectrum of the current compromise the data for CR. The larger the current density ( $i_{corr}$ ), the higher the peaks. The EFM spectra of CS in 1 M HCl in the absence and presence of various concentrations are shown in Fig. 10 and the results are displayed in Table 8. As the inhibitor concentration rose, the  $i_{corr}$  decreased. Theoretical values are equivalent to testing-derived causality factors<sup>71</sup>.

## Surface investigations

### SEM examination

C-steel bars were immersed in a corrosive medium containing 300 ppm Furosemide at 298 K for 24 h to study surface morphology<sup>72</sup>. The effect of Furosemide addition on the surface of C steel is depicted in Fig. 11. Figure 11b,c depict the surface of C-steel in corrosive conditions without and with the addition of Furosemide, respectively, demonstrating the production of rust on the metal surface as a result of exposure to corrosive medium oxygen, water molecules, and chloride ions, as described in Eqs. (12) and (13):



The figure shows the construction of a shielding adsorbed layer on the surface of the C-steel.

### AFM examination

AFM was employed to measure surface image evidence at the nano-to-micro-scale<sup>73</sup>. The morphologies of CS dissolution in a 1.0 M HCl corrosive solution in the absence and presence of a 300 ppm inhibitor are shown in Fig. 12. The root mean square roughness (Rq) determines the average lines, and the average roughness (Ra) explains the mean deviations of all roughness images. Significant corrosion and increased roughness are visible in an AFM image of the CS specimen in 1.0 M HCl. The measured IE% calculated from ML and electrochemical performances were validated and matched with roughness data. The data in Table 9 reveal that in the presence of Furosemide, the metal surface is smoothed due to the adsorption of the compound through the active center sites.

### Examination of X-ray photoelectron spectroscopy (XPS)

It is an ideal system for predicting the adsorbed atoms on the metal surface. XPS investigation of carbon steel after immersion in 1 M HCl with 300 ppm Furosemide at 25 °C for particular atoms such as C, O, N, and Fe. The obtained results are displayed in Figs. 13 and 14. The position of the peak of this curve represents the adsorbed atoms and the intensity represents the concentration of the adsorbed element<sup>74-77</sup>. The C steel bar is released in a corrosive medium (1 M HCl) for 24 h in the presence of 300 ppm of the investigated compound. Table 10 summarizes the results of the data analysis.

### FT-IR spectroscopy

FT-IR spectra, as shown in Fig. 15, illustrate the functional groups of the solutions and their behaviour on the metal surface following adsorption with amazing precision. Table 11 shows how the FTIR results could be interpreted. Figure 15 depicts the FT-IR spectra of pure inhibitor and layers formed on CS samples after dipping in 1.0 M HCl for a day in the presence of 300 ppm Furosemide. When the spectra of the inhibitor solution and the spectra of the CS surface after immersion are compared, the two spectra have identical features, suggesting that the compounds were adsorbed on the CS<sup>78</sup>. The results demonstrate the interference mechanism between the inhibitor and the carbon steel surface. The shifting and removal of peaks in the spectrum after immersion demonstrated that the inhibitor interacted with the carbon steel surface via functional groups.

## Quantum chemistry and statistics parameters

Figure 16 represents the HOMO and LUMO electronic densities distributions of the Furosemide compound. According to the literature, the inhibitor molecule's  $E_{HOMO}$  is a direct indication of its tendency to donate electrons to acceptor atoms, whereas  $E_{LUMO}$  is a measure of taking electrons into its LUMO from a compatible donor molecule.  $\Delta E_{gap}$  indicates the difference between  $E_{LUMO}$  and  $E_{HOMO}$ . It is widely known that low values of  $\Delta E_{gap}$  afford good inhibitory performances, since the energy for removing an electron from the final occupied orbital is low<sup>79</sup>. The low value of  $\Delta E_{gap}$  for the investigated inhibitor reveals the strong inhibition efficacy of the examined

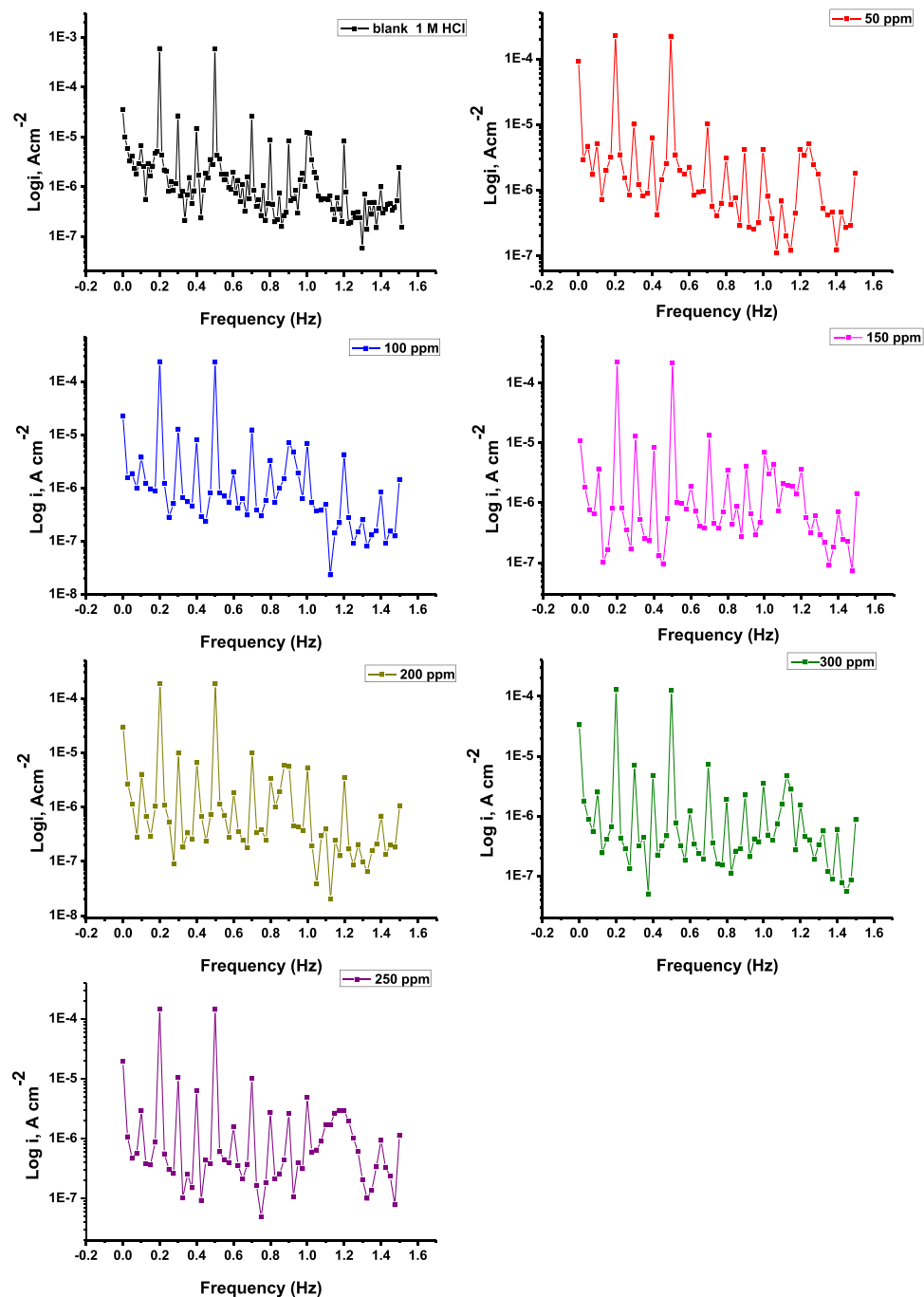


**Figure 10.** EFM spectra for corrosion of the CSI surface in 1.0 M HCl with and without various concentrations of Furoseme compound at 298 K.

compound, which indicates good adsorption of the explored inhibitor on the mild steel surface<sup>79</sup>. Equation (14) is used to estimate the fraction of electrons transported ( $\Delta N$ ) from an inhibitor molecule to the metallic surface:

$$\Delta N = (\chi_{\text{Fe}} - \chi_{\text{inh}})/2(\eta_{\text{Fe}} + \eta_{\text{inh}}) \quad (14)$$

whereas  $\chi_{\text{Fe}}$  and  $\chi_{\text{inh}}$  represent the overall electronegativity of the iron atom and the inhibitor molecule, respectively,  $\eta_{\text{Fe}}$  and  $\eta_{\text{inh}}$  imply the absolute hardness of the iron atom and the inhibitor molecule.  $\chi_{\text{Fe}}$  is  $7 \text{ eV mol}^{-1}$  and  $\eta_{\text{Fe}}$  iron is  $0 \text{ eV mol}^{-1}$ .

These quantities are directly associated with the electron affinity (A) and ionization potential (I) of the relevant chemical systems shown below. Electronegativity ( $\chi$ ) and hardness can be calculated from Eqs. (15) and (16), respectively

Compound	Conc. (ppm)	$i_{corr}$ ( $\mu\text{A cm}^{-2}$ )	$-\beta_c$ (mv dec $^{-1}$ )	$\beta_a$ (mV dec $^{-1}$ )	CF-2	CF-3	$k_{corr}$ (mpy)	$\theta$	IE %
Blank	0	929	191	135	1.8	3.5	480	–	–
Inhibitor	50	400	102	80	1.7	3.2	215	0.569	56.9
	100	380	100	83	2.4	3.1	200	0.591	59.1
	150	280.2	103	84	1.8	3.0	148.1	0.698	69.8
	200	262.1	97	78	1.6	2.8	148.1	0.717	71.7
	250	239.5	97	80	1.8	3	124.7	0.742	74.2
	300	210.6	87	72	1.7	3.1	110.3	0.773	77.3

**Table 8.** Electrochemical parameters from EFM of the CS in 1.0 M HCl without and with various doses of Furosemide at 298 K.

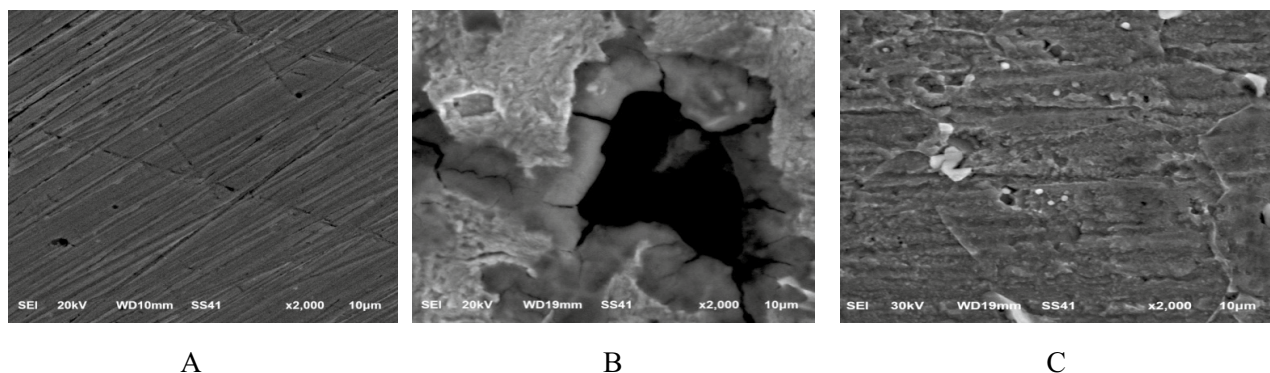


**Figure 11.** SEM micrographs of (CS) samples (A) pure CS sample, (B) CS in 1.0 M HCl solution after the immersion for 24 h at 298 K (C) CS immersed in 1.0 M HCl solution with 300 ppm of Furosemide for 24 h at 298 K.

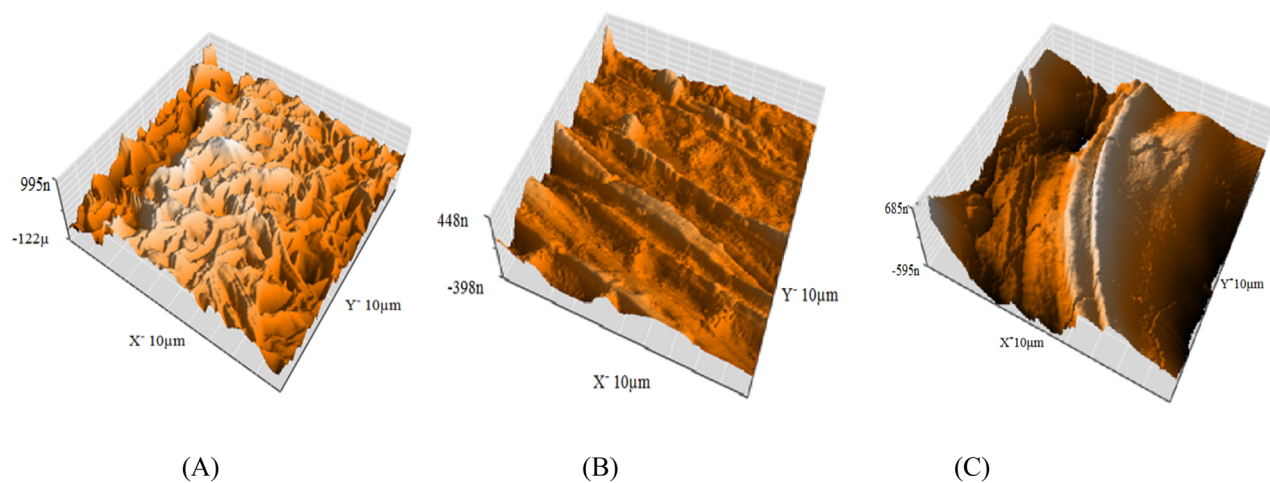


**Figure 12.** Three-dimensional (3D) AFM images of the CS samples, (A) before involvement in acid, (B) the CS sample immersed in 1.0 M HCl for 24 h at 298 K (C) the CS sample immersion in 1.0 M HCl with 300 ppm of the Furosemide for 24 h at 298 K.

Specimen	Average roughness (Ra) nm	RMS roughness (Rq) nm
(CS) metal surface (pure)	48.7	63.0
(CS) metal surface + 1.0 M HCl (blank)	271.7	335.6
(CS) metal surface + Furosemide compound	108.2	141.8

**Table 9.** AFM roughness measurements of the (CS) samples without and with 300 ppm of from the investigated compound after immersion in 1.0 M HCl for 24 h at 298 K.

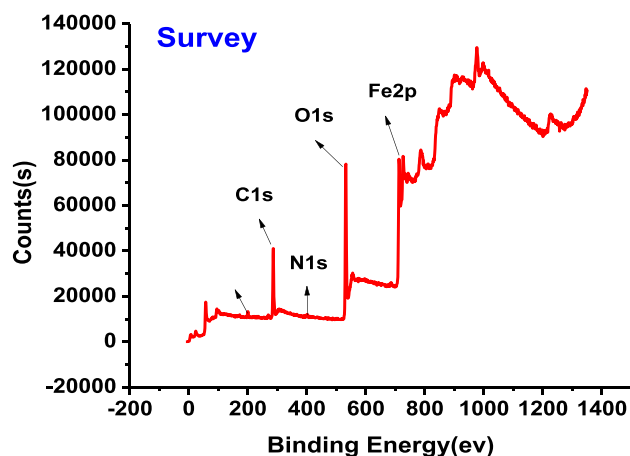


**Figure 13.** The XPS survey spectrum results of Furosemide compound adsorbed on the CS in 1 M HCl at 298 K.

$$\chi = (I + A)/2 \quad (15)$$

and

$$\eta = (I - A)/2 \quad (16)$$

Using Koopman's theorem,  $I = -E_{\text{HOMO}}$  and  $A = -E_{\text{LUMO}}$ . It has been found that a value of  $\Delta N$  smaller than 3.6 indicates higher inhibitor efficacy due to the inhibitor's electron-donating capacity to the iron surface<sup>80</sup>. The computed  $\Delta N$  value of 1.437 supports the experimental interpretations. Figure 16 depicts a schematic illustration of Furosemide inhibition.

Table 12 provides quantum chemical characteristics that predict the relationship between the molecular construction of inhibitor particles and their effect against CS corrosion, in addition to the major effect on electronic interference between CS and inhibitor solution.

One of the most vital features, which is related to the polarity of the inhibitive particle, is the dipole moment<sup>81</sup>. Table 12 displays that the calculated value of the dipole moment ( $\mu_{\text{inh}} = 6.18$  Debye) for the studied molecule is higher than that of  $\text{H}_2\text{O}$  ( $\mu_{\text{H}_2\text{O}} = 1.88$  Debye). The number of inhibitory sites on the metal surface in the corrosive environment is increased by this high dipole moment value. As a result, the strong dipole–dipole interactions between the inhibitor and the metal surface, as demonstrated in Table 12 and Fig. 16, are responsible for the inhibitor's high dipole moment. Certain parameters, such as global hardness ( $\eta$ ) and softness ( $\sigma$ ), are linked to the molecule's selectivity and reactivity. As per the Lewis theory of acid/base and Pearson's hard/soft acids and bases<sup>82</sup>, more reactive and greater  $\Delta E$  values are associated with hard molecules. Based on Table 12, it can be inferred that Furosemide has a greater  $\sigma$  value, indicating a softer nature. Furosemide would therefore be more likely to provide electrons to CS.

### Molecular electrostatic potential (MEP)

The molecular electrostatic potential (MEP) is used to determine a species' relative reactivity under nucleophilic and electrophilic attack. DFT calculations were used to analyze the compound's MEP surface, using the optimized structure and B3LYP/6-31Gp(d,p) basis set. MEP is used to examine the relationship between a compound's structure and its physicochemical properties, as well as interactions with metal surfaces. MEP modeling was recognized as a highly effective method<sup>83</sup>. Figure 17 depicts the electrostatic potential surface mapped for Furosemide. The MEP chart shows discrete zones with negative and positive potential. The MEP chart depicts how potential varies with colour is transite from blue to green, yellow, orange, and red<sup>84</sup>. The polarization effect is plainly seen in the compound. The negative potential regions of the MEP are confined over the electronegative atoms (oxygen, nitrogen, and sulfur). The green–blue regions represent positive potentials, indicating they receive electrons from the metal surface. Conversely, the red–yellow zones show negative potentials associated with electrophilic and nucleophilic performance.

### Mechanism of inhibition

The efficacy of the investigated compound as an inhibitor for CS corrosion in 1 M HCl is examined. Concentration, the number of active sites and their charge densities, molecule mass, and environmental stability are factors that influence the inhibition process<sup>85–88</sup>. In a 1 M HCl solution, the examined compound could exist as neutral molecules or in protonated form (cations). The compound may adsorb on the CS/HCl interface via one or more of the following mechanisms: (1) electrostatic interaction of the protonated form with adsorbed chloride ions; (2) donor–acceptor interactions between the electrons of the aromatic ring and vacant d orbitals of surface iron atoms; and (3) interaction between unshared electron pairs of inhibitor heteroatoms and vacant d orbitals of iron surface atoms. In one approach, the neutral inhibitor may be adsorbed on the CS surface via the chemisorption

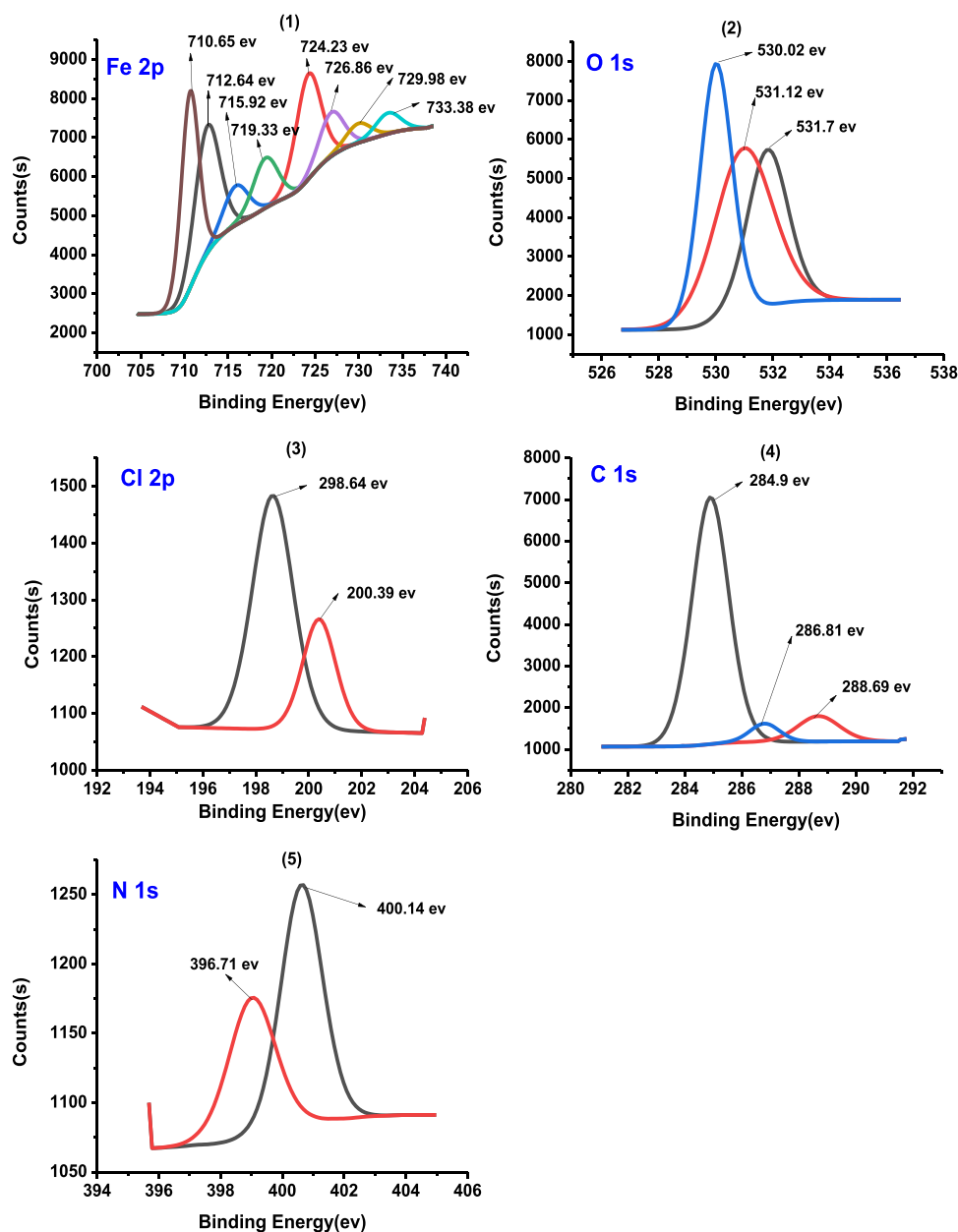


**Figure 14.** High-resolution X-ray photoelectron profiles of (1) Fe 2p, (2) O 1s, (3) Cl 2p, (4) C 1s and (5) N 1s for (CS) in presence of 300 ppm furosemide compound in 1 M HCl at 298 K.

mechanism<sup>89</sup>. The inhibitor molecules can also adsorb on the surface via donor–acceptor interactions between the p-electrons of the heterocyclic ring and the surface iron's unoccupied d orbitals. In another way, because it is well known that the CS surface bears a positive charge in acid solution, the protonated inhibitor finds it difficult to approach the positively charged CS surface due to electrostatic repulsion. Because the CS surface is positively charged, anions ( $\text{Cl}^-$  ions) in an aqueous hydrochloric acid solution are adsorbed on it. The CS surface becomes negatively charged after  $\text{Cl}^-$  ion adsorption. As a result of electrostatic interactions with the  $\text{Cl}^-$  ions already adsorbed on the surface of CS, the protonated positively charged form of inhibitor is adsorbed on the surface of CS. As a result, adsorbed  $\text{Cl}^-$  ions and protonated inhibitor work together. Figure 18 shows a graphic representation of the adsorption of the investigated inhibitor molecule on the CS surface.

## Conclusions

1. Furosemide is safe for people; it can be used as a green corrosion inhibitor to protect CS from corrosion in 1 M HCl.
2. As Furosemide medication concentrations are increased, the efficiency of corrosion inhibition improves, reaching 90.5% at 300 ppm and 318 K.

Scan type	Binding energies peaks (ev)	Peak refers to
Fe 2p	710.65	Fe 2p3/2 (Fe <sup>2+</sup> oxide state of FeO)
	712.64	Fe 2p3/2 (Fe <sup>3+</sup> oxide state of Fe <sub>2</sub> O <sub>3</sub> or FeCl <sub>3</sub> )
	715.92	Fe 2p3/2 (Fe <sup>2+</sup> satellite)
	719.33	Fe 2p3/2 (Fe <sup>3+</sup> satellite)
	724.23	Fe 2p1/2 (Fe <sup>2+</sup> oxide state of FeO)
	726.86	Fe 2p1/2 (Fe <sup>3+</sup> oxide state of Fe <sub>2</sub> O <sub>3</sub> )
	729.98	Fe 2p1/2 (Fe <sup>2+</sup> satellite)
	733.38	Fe 2p1/2 (Fe <sup>3+</sup> satellite)
O 1s	530.02	Fe <sub>2</sub> O <sub>3</sub>
	531.12	C-O
	531.7	C=O or C-O-C
Cl 2p	198.64	Cl 2p3/2
	200.39	Cl 2p1/2
C 1s	284.4	C-C
	285.9	C-(O, N) or C-Cl bond in inhibitor
	288.6	O-C=O
N 1s	396.71	(Fe-N-C) and (-C=N)
	400.14	(-N-H)

**Table 10.** Lists the binding energies of various surveys and the expected bonds for each.

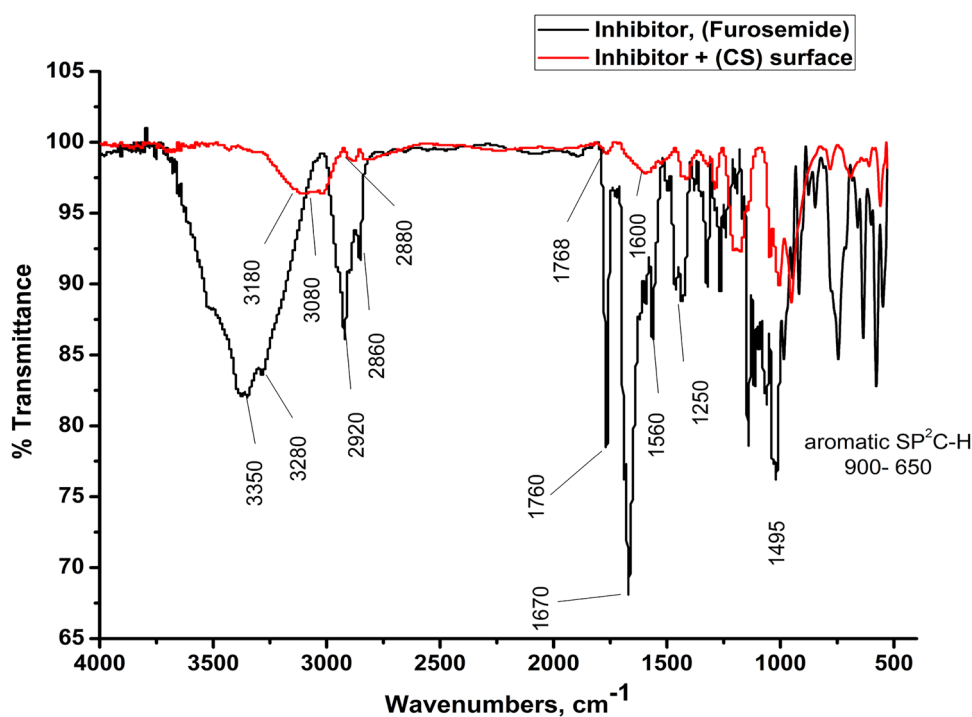


**Figure 15.** FT-IR spectra of pure Furosemide and of CS metal surface in 1.0 M HCl with 300 ppm of Furosemide compound for 6 h at 298 K.

- The potentiodynamic polarisation investigations revealed that  $E_{\text{corr}}$  values are slightly affected, indicating that the Furosemide drug inhibitor is a mixed-type inhibitor.
- The adsorption of Furosemide medication on the Cs surface, as well as the formation of a barrier film that isolates the metal from corrosive environments prevent corrosion.
- The inhibitor's adsorption followed the Temkin adsorption isotherm.
- According to the studies from different procedures that are in good agreement with one another, Furosemide medicine prevents CS corrosion in 1 M HCl and delays the process of iron breakdown in this environment.
- The quantum chemical description of the inhibitory activity of Furosemide confirms the experimental data.

Comp	Solution peaks and frequencies (cm <sup>-1</sup> )	Frequencies refer to	Shifting, missing and new peaks and frequencies (cm <sup>-1</sup> ) after adsorption
Furosemide	3350, 3280	Stretching primary amine -NH <sub>2</sub>	Missed
	-	Stretching alcoholic for solvent O-H	3200
	-	Stretching secondary amine -NH <sub>2</sub>	3130
	2920	Carboxylic acidic stretching O-H	2882
	2850	Stretching SP <sup>3</sup> -C-H	2815
	1766	Stretching carboxylic acidic stretching O-H group (-C=O)	1768
	1688	Stretching (C=C)	Missed
	1560	Bending -N-H-	1597
	1150	Alkoxy C-O	1150
	900-650	Aromatic SP <sup>2</sup> C-H bending	950-550
	790	Ortho di-substituted	785
	780	Para di-substituted	770
	659	Meta di-substituted	691

**Table 11.** FTIR spectra of Furosemide pure solutions and the spectra of the CS surface after inhibitor adsorption CS metal surface in 1.0 M HCl with (300 ppm) of Furosemide compound for 6 h at 298 K.

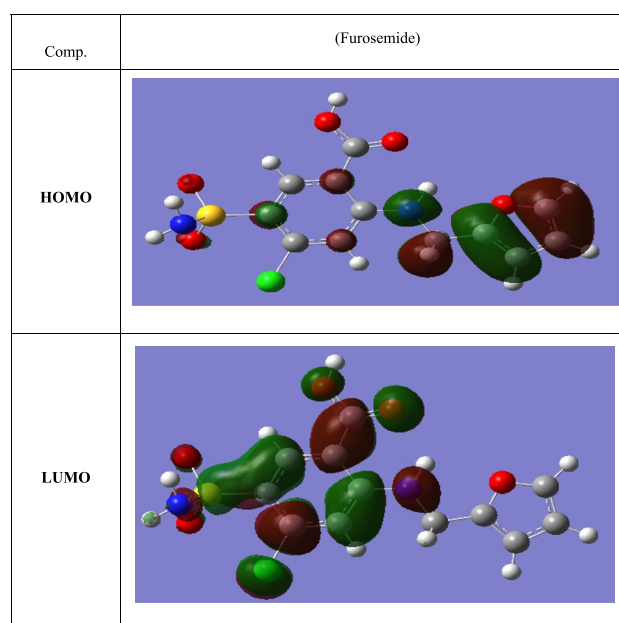


**Figure 16.** HOMO and LUMO electronic densities distributions of Furosemide compound.

Parameter	Compound (Furosemide)
$E_{HOMO}$ (eV)	-6.11
$E_{LUMO}$ (eV)	-2.03
$\Delta E_{gap}$ (eV)	4.08
$\mu$ (debye)	6.18
$I = -E_{HOMO}$	6.11
$A = -E_{LUMO}$	2.03
$\chi = (I + A)/2$	4.07
$\eta = I - A/2$	2.04
$\sigma = 1/\eta$	0.49
$\Delta N$	1.437

**Table 12.** Quantum chemical parameters for Furosemide compound in liquid phase.



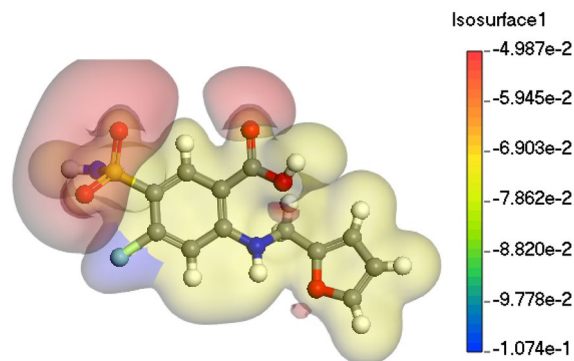


**Figure 17.** MEP surface of Furosemide compound.

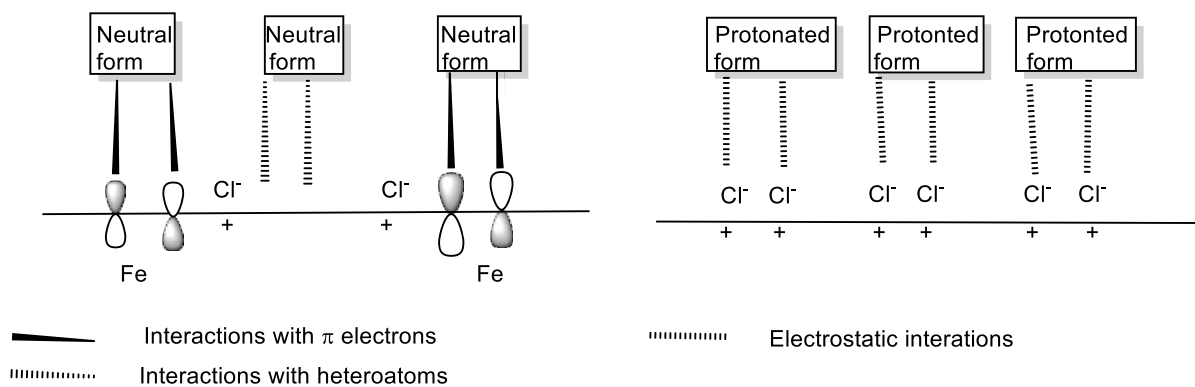


**Figure 18.** Representation of the different modes of adsorption of Furosemide drug on the CS surface.

Inhibitor	Optimum dose	Metal substrate	Corrosive media	Temp	Inhibition efficiency (%)	References
Furosemide	300 ppm	C-steel	1 M HCl	298 K	87.6	This study
Furosemide	300 ppm	Zinc	2 M HCl	298 K	81.32	<sup>90</sup>
Furosemide	$14 \times 10^{-4}$ M	Mild steel	1 M HCl	303 K	84.73	<sup>91</sup>
Hydrochlorothiazide	$15 \times 10^{-5}$ M	C- steel	2 M HCl	303 K	81.8	<sup>92</sup>
Acyl hydrazide containing sulfonamide moiety (p-TSAH)	$1 \times 10^{-3}$ M	Mild steel	1 M HCl	298 K	93.73	<sup>93</sup>

**Table 13.** Comparison of our outcomes with previously reported studies on the employment of Furosemide and its derivatives as anti-corrosive agents.

Comparison between the results obtained from this study and other studies on Furosemide and its related compounds are illustrated in Table 13.

## Data availability

The following instruments were used in this study. Potentiostat/galvanostat/ZRA (Gamry Reference 3000) in Faculty of Science, Port Said University. SEM, The analysis was performed using a Scanning Electron Microscope (JEOL JSM-5500, Japan). Faculty of Agriculture, Mansoura University, Egypt. AFM device model is Thermo Fisher Nicolet IS10 (scanning probe microscope) was employed at Nanotechnology Laboratory, Faculty of Engineering Mansoura University, Egypt. The XPS test was performed using K-ALPHA (Thermo Fisher Scientific, USA). Central Metallurgical Research Institute (CMRDI), Helwan, Egypt. FTIR spectra were performed using PerkinElmer 1600 spectrophotometer, Faculty of Pharmacy Mansoura University, Egypt.

Received: 28 January 2024; Accepted: 2 April 2024

Published online: 20 April 2024

## References

- Bentiss, F., Lagrenée, M. & Traisnel, M. 2, 5-bis (n-pyridyl)-1, 3, 4-oxadiazoles as corrosion inhibitors for mild steel in acidic media. *Corrosion* **56**, 733 (2000).
- Mehdaoui, R. *et al.* Corrosion inhibition of carbon steel in hydrochloric acid solution by some synthesized surfactants from petroleum fractions. *Res. Chem. Intermed.* **42**, 5509–5526 (2016).
- Nnabuk Eddy, O., Momoh-Yahaya, H. & Oguzie Emeka, E. Theoretical and experimental studies on the corrosion inhibition potentials of some purines for aluminum in 0.1 M HCl. *J. Adv. Res.* **6**, 203–217 (2015).
- Sadeghi Meresht, E., Shahrabi Farahani, T. & Neshati, J. 2-Butyne-1, 4-diol as a novel corrosion inhibitor for API X65 steel pipeline in carbonate/bicarbonate solution. *Corros. Sci.* **54**, 36–44 (2012).
- Gopiraman, M., Selvakumaran, N., Kesavan, D. & Karvembu, R. Adsorption and corrosion inhibition behaviour of N-(phenylcarbamothioyl) benzamide on mild steel in acidic medium. *Prog. Org. Coat.* **73**, 104–111 (2012).
- Hosseini, M., Mertens, S. F., Ghorbani, M. & Arshadi, M. R. Asymmetrical Schiff bases as inhibitors of mild steel corrosion in sulphuric acid media. *Mat. Chem. Phys.* **78**, 800–808 (2003).
- Abdallah, M., El-Dafrawy, A. M., Sobhi, M., Elwahy, A. H. M. & Shaaban, M. R. Corrosion inhibition of carbon steel in sulphuric acid solutions by novel bisaminothiazole derivatives: Chemical, electrochemical and DFT Studies. *Int. J. Electrochem. Sci.* **9**, 2186–2207 (2014).
- Fouda, A. S., El-Sayyad, S. A. & Abdallah, M. N-3-hydroxyl-2-naphthoyle hydrazone derivatives as inhibitors for corrosion of carbon steel in H<sub>2</sub>SO<sub>4</sub> acid solution. *Anti-Corros. Methods Mat.* **58**, 63–69 (2011).
- Sobhi, M., Abdallah, M. & Hfaez, E. Some polysorbate compounds as corrosion inhibitors for carbon steel in hydrochloric acid. *J. Adv. Chem.* **5**, 830–838 (2009).
- Abdallah, M., Asghar, B. H., Zaaafarany, I. & Sobhi, M. Synthesis of some aromatic nitro compounds and its applications as inhibitors for corrosion of carbon steel in hydrochloric acid solution. *Pro. Methods Phys. Chem. Surf.* **49**, 485–491 (2013).
- Fouda, A. S., Abdallah, M. & Medhat, M. Some Schiff base compounds as inhibitors for corrosion of carbon steel in acidic media. *Pro. Methods Phys. Chem. Surf.* **48**, 477–486 (2012).
- Issaadi, S. *et al.* Novel thiophene symmetrical Schiff base compounds as corrosion inhibitor for mild steel in acidic media. *Corros. Sci.* **53**, 1484–1488 (2011).
- Abdallah, M., Zaaafarany, I., Khairou, K. S. & Sobhi, M. Inhibition of carbon steel corrosion by iron (III) and imidazole in sulfuric acid. *Int. J. Electrochem. Sci.* **7**, 1564–1579 (2012).
- Radojčić, I., Berković, K., Kovač, S. & Vorkapić-Furač, J. J. C. S. Natural honey and black radish juice as tin corrosion inhibitors. *Corros. Sci.* **50**, 1498–1504 (2008).
- Oguzie, E. E. Evaluation of the inhibitive effect of some plant extracts on the acid corrosion of mild steel. *Corros. Sci.* **50**, 2993–2998 (2008).
- Olusegun Abiola, K., Otaigbe, J. O. E. & Kio, O. J. *Gossypium hirsutum* L. extracts as green corrosion inhibitor for aluminum in NaOH solution. *Corros. Sci.* **51**, 1879–1881 (2009).
- Okafor, P. C. & Zheng, Y. G. Synergistic inhibition behaviour of methylbenzyl quaternary imidazoline derivative and iodide ions on mild steel in H<sub>2</sub>SO<sub>4</sub> solutions. *Corros. Sci.* **51**, 850–859 (2009).
- Abdallah, M. *et al.* Enhancing the inhibition and adsorption performance of SABIC iron corrosion in sulfuric acid by expired vitamins. Experimental and computational approach. *RSC Adv.* **11**, 17092 (2021).
- Zhang, Z., Chen, S., Li, Y., Li, S. & Wang, L. A study of the inhibition of iron corrosion by imidazole and its derivatives self-assembled films. *Corros. Sci.* **51**, 291–300 (2009).
- Mahdavian, M. & Attar, M. M. Electrochemical behaviour of some transition metal acetylacetonate complexes as corrosion inhibitors for mild steel. *Corros. Sci.* **51**, 409–414 (2009).
- Liu, X., Okafor, P. C. & Zheng, Y. G. The inhibition of CO<sub>2</sub> corrosion of N80 mild steel in single liquid phase and liquid/particle two-phase flow by aminoethyl imidazoline derivatives. *Corros. Sci.* **51**, 744–751 (2009).
- Arslan, T., Kandemirli, F., Ebeso, E. E., Love, I. & Alemu, H. Quantum chemical studies on the corrosion inhibition of some sulphonamides on mild steel in acidic medium. *Corros. Sci.* **51**, 35–47 (2009).
- Liu, F. G., Du, M., Zhang, J. & Qiu, M. Electrochemical behavior of Q235 steel in saltwater saturated with carbon dioxide based on new imidazoline derivative inhibitor. *Corros. Sci.* **51**, 102–109 (2009).
- Roque, J. M., Pandiyan, T., Cruz, J. & García-Ochoa, E. DFT and electrochemical studies of tris (benzimidazole-2-ylmethyl) amine as an efficient corrosion inhibitor for carbon steel surface. *Corros. Sci.* **50**, 614–624 (2008).
- Chikh, Z. A. *et al.* Electrochemical and analytical study of corrosion inhibition on carbon steel in HCl medium by 1, 12-bis (1, 2, 4-triazolyl) dodecane. *Corros. Sci.* **47**, 447–459 (2005).
- Merimi, C. *et al.* Acetylsalicylic acid as an environmentally friendly corrosion inhibitor for carbon steel XC48 in chloride environment. *J. Mol. Str.* **1278**, 134883 (2023).
- Salem, A. M., Wahba, A. M., El Hossiany, A. & Fouda, A. S. Experimental and computational chemical studies on the corrosion inhibitive properties of metamizole sodium pharmaceutical drug compound for CS in hydrochloric acid solutions. *J. Ind. Chem. Soci.* **99**, 100778 (2022).
- Shojaee, S., Zandi, M. S. & Rastakhiz, N. The effect of tetracycline drug as a green corrosion inhibitor for carbon steel in HCl media. *J. Ind. Chem. Soci.* **99**, 100700 (2022).
- Sh Mahmoud, Z. *et al.* Study the inhibition effect of amoxicillin drug for corrosion of carbon steel in saline media. *Bagh. Sci. J.* **19**, 0121 (2022).
- Mehmeti, V. Nystatin drug as an effective corrosion inhibitor for mild steel in acidic media—an experimental and theoretical study. *Corros. Sci. Technol.* **21**(1), 21–31 (2022).
- Deyab, M. A., El-Shamy, O. A., Thabet, H. K. & Ashmawy, A. M. Electrochemical and theoretical investigations of favipiravir drug performance as ecologically benign corrosion inhibitor for aluminum alloy in acid solution. *Sci. Rep.* **13**, 8680 (2023).

32. Abeng, F. E. *et al.* Corrosion inhibition of API 5L X-52 pipeline steel in oilfield acidizing solution by gentamicin and sulfamethoxazole: Experimental, plane-wave density functional theory (PWDF) and the generalized-gradient approximation (GGA) simulations. *J. Adhes. Sci. Tech.* **36**, 2438–2461 (2022).
33. Nathiya, R. S., Perumal, S., Murugesan, V. & Raj, V. Expired drugs: Environmentally safe inhibitors for aluminium corrosion in 1 M H<sub>2</sub>SO<sub>4</sub>. *J. Bio-Tribo-Corros.* **4**, 4 (2018).
34. Singh, A. K. & Quraishi, M. A. Effect of Cefazolin on the corrosion of mild steel in HCl solution. *Corros. Sci.* **52**, 152–160 (2010).
35. Ikeuba, A. I. *et al.* Experimental and theoretical evaluation of aspirin as a green corrosion inhibitor for mild steel in acidic medium. *Res. Chem.* **4**, 100543 (2022).
36. Fouda, A. S., Shalabi, K. & E-Hossiany, A. Moxifloxacin antibiotic as green corrosion inhibitor for carbon steel in 1 M HCl. *J. Bio-Tribo-Corros.* **2**, 1–13 (2016).
37. Usman, B., Maarof, H., Abdallah, H. H. & Aziz, M. Inhibition performance of mild steel corrosion in acidic media using 2-thiophene acetyl chloride. *Bayero J. Pure Appl. Sci.* **10**, 590–595 (2017).
38. Obot, I. B., Obi-Egbedi, N. O., Umoren, S. A. & Ebenso, E. E. Adsorption and kinetic studies on the inhibition potential of flucanazole for the corrosion of Al in HCl solution. *Chem. Eng. Com.* **198**, 711–725 (2011).
39. Motaleb, M. A. & Nassar, M. Y. Preparation, molecular modeling and biodistribution of <sup>99m</sup>Tc-phytochlorin complex. *J. Radioanal. Nucl. Chem.* **299**, 1759–1766 (2014).
40. Abd-El Rehim, S. S., Ibrahim, M. A. M. & Khalid, K. F. The inhibition of 4-(2-amino-5-methylphenylazo)antipyrine on corrosion of mild steel in HCl solution. *Mater. Chem. Phys.* **70**, 268–273 (2001).
41. AbdelHameed, R. S. *et al.* Expired dulcolax drug as corrosion inhibitor for low carbon steel in acidic environment. *Int. J. Electrochem. Sci.* **17**, 1–16 (2022).
42. Duca, D. A., Dan, M. L. & Vaszilcsin, N. Expired domestic drug-paracetamol-as corrosion inhibitor for carbon steel in acid media. *IOP Conf. Ser. Mat. Sci. Eng.* **416**, 012043 (2018).
43. Abdallah, M. *et al.* Appraisal of adsorption and inhibition effect of expired micardis drug on aluminum corrosion in hydrochloric acid solution. *Int. J. Electrochem. Sci.* **17**, 220462 (2022).
44. Alamry, K. A., Khan, A., Aslam, J., Hussein, M. A. & Aslam, R. Corrosion inhibition of mild steel in hydrochloric acid solution by the expired Ampicillin drug. *Sci. Rep.* **13**, 6724 (2023).
45. Geethamani, P., Narmatha, M., Dhanalakshmi, R., Aejitha, S. & Kasthuri, P. K. Corrosion inhibition and adsorption properties of mild steel in 1 M hydrochloric acid medium by expired amroxol drug. *J. Bio Tribo Corros.* **5**, 16 (2019).
46. Alfakeer, M., Abdallah, M. & Fawzy, A. Corrosion inhibition effect of expired ampicillin and flucloxacillin drugs for mild steel in aqueous acidic medium. *Int. J. Electrochem. Sci.* **15**, 3283–3297 (2020).
47. Tajabadipour, H., Mohammadi-Manesh, H. & Shahidi-Zandi, M. Experimental and theoretical studies of carbon steel corrosion protection in phosphoric acid solution by expired lansoprazole and rabeprazole drugs. *J. Indian Chem. Soc.* **99**, 100285 (2022).
48. Solmaz, R. Investigation of adsorption and corrosion inhibition of mild steel in hydrochloric acid solution by 5-(4-Dimethylaminobenzylidene) rhodanine. *Corros. Sci.* **79**, 169–176 (2014).
49. Singh, D. D. N., Chaudhary, R. S., Prakash, B. & Agarwal, C. V. Inhibitive efficiency of some substituted thioureas for the corrosion of aluminium in nitric acid. *Bri. Corros. J.* **14**, 235–239 (1979).
50. Sudhish, K. & Quraishi, M. A. Sh 4-Substituted anilinomethylpropionate: New and efficient corrosion inhibitors for mild steel in hydrochloric acid solution. *Corros. Sci.* **51**, 1990–1997 (2009).
51. Fouda, A. S., Al-Sarawy, A. A. & El-Katori, E. E. Pyrazolone derivatives as corrosion inhibitors for C-steel in hydrochloric acid solution. *Des* **201**, 1–13 (2006).
52. Masroor, Sh. & Mobin, M. Non-ionic surfactant as corrosion inhibitor for aluminium in 1 M HCl and synergistic influence of Gemini surfactant. *Chem. Sci. Rev. Lett.* **3**, 33–48 (2014).
53. El-desoky, A. M., Fouda, A. S. & Nabih, A. Inhibitive, adsorption, synergistic studies on copper corrosion in nitric acid solutions by some organic derivatives. *Adv. Mater. Corros.* **2**, 1–15 (2013).
54. Lakshmi, S. G., Tamilselvi, S., Rajendran, N., Babi, M. A. K. & Arivuoli, D. Electrochemical behaviour and characterisation of plasma nitrided Ti-5Al-2Nb-1Ta orthopaedic alloy in Hanks solution. *Sur. Coat. Tech.* **182**, 287–293 (2004).
55. Xianghong, L., Shuduan, D., Guannan, M. & Fazhon, Y. Inhibition effect of nonionic surfactant on the corrosion of cold rolled steel in hydrochloric acid. *Corros. Sci.* **50**, 420–430 (2008).
56. Fouda, A. S., Mekkia, D. & Badr, A. H. Extract of *Camellia sinensis* as green inhibitor for the corrosion of mild steel in aqueous solution. *J. Kor. Chem. Soci.* **57**, 264–271 (2013).
57. Abdallah, M. Rhodanine azosulpha drugs as corrosion inhibitors for corrosion of 304 stainless steel in hydrochloric acid solution. *Corros. Sci.* **44**, 717–728 (2002).
58. Al-Otaibi, M. S. *et al.* Corrosion inhibitory action of some plant extracts on the corrosion of mild steel in acidic media. *Arab. J. Chem.* **7**(3), 340–346 (2014).
59. Shaban, S. M. *et al.* Corrosion inhibition and surface examination of carbon steel 1018 via N-(2-(2-hydroxyethoxy)ethyl)-N,N-dimethyloctan-1-aminium bromide in 1.0 M HCl. *J. Mol. Struct.* **1227**, 129713 (2021).
60. Ahamad, I., Prasad, R. & Quraishi, M. A. Thermodynamic, electrochemical and quantum chemical investigation of some Schiff bases as corrosion inhibitors for mild steel in hydrochloric acid solutions. *Corros. Sci.* **52**, 933–942 (2010).
61. Lgaz, H. *et al.* Evaluation of 2-mercaptobenzimidazole derivatives as corrosion inhibitors for mild steel in hydrochloric acid. *Metals* **10**, 357 (2020).
62. Qu, Q., Jiang, S., Bai, W. & Li, L. Effect of ethylenediamine tetraacetic acid disodium on the corrosion of cold rolled steel in the presence of benzotriazole in hydrochloric acid. *Electrochim. Acta* **52**, 6811–6820 (2007).
63. Hsu, C. H. & Florian, M. Concerning the conversion of the constant phase element parameter Y<sub>0</sub> into a capacitance. *Corrosion* **57**, 747–748 (2001).
64. Behpour, M., Ghoreishi, S. M., Mohammadi, N., Soltani, N. & Salavati-Niasari, M. Investigation of some Schiff base compounds containing disulfide bond as HCl corrosion inhibitors for mild steel. *Corros. Sci.* **52**, 4046–4057 (2010).
65. Yildiz, R., Arslanhan, S., Döner, A. & FiratBaran, M. Corrosion behavior of mild steel in 1 M HCl with *Cyclotrichium niveum* as a green inhibitor. *Mater. Chem. Phys.* **312**, 128654 (2024).
66. Özcan, M., Dehri, I. & Erbil, M. Organic sulphur-containing compounds as corrosion inhibitors for mild steel in acidic media: Correlation between inhibition efficiency and chemical structure. *Appl. Surf. Sci.* **236**, 155–164 (2004).
67. Solmaz, R., Kardeş, G., Çulha, M., Yazıcı, B. & Erbil, M. Investigation of adsorption and inhibitive effect of 2-mercaptothiazoline on corrosion of mild steel in hydrochloric acid media. *Electrochim. Acta* **53**, 5941–5952 (2008).
68. Erbil, M. The determination of corrosion rates by analysis of AC impedance diagrams. *Chim. Acta Turcica* **1**, 59–70 (1988).
69. Benali, O., Larabi, L., Mekelleche, S. M. & Harek, Y. Influence of substitution of phenyl group by naphthyl in a diphenylthiourea molecule on corrosion inhibition of cold-rolled steel in 0.5 M H<sub>2</sub>SO<sub>4</sub>. *J. Mater. Sci.* **41**, 7064–7073 (2006).
70. Bosch, R. W., Hubrecht, J., Bogaerts, W. F. & Syrett, B. C. Electrochemical frequency modulation: A new electrochemical technique for online corrosion monitoring. *Corrosion* **57**, 60–70 (2001).
71. Noor, E. A. & Al-Moubaraki, A. H. Thermodynamic study of metal corrosion and inhibitor adsorption processes in mild steel/1-methyl-4 [4'(-X)-styryl] pyridinium iodides/hydrochloric acid systems. *Mat. Chem. Phys.* **110**, 145–154 (2008).
72. Prabhu, R. A., Venkatesha, T. V., Shanbhag, A. V., Kulkarni, G. M. & Kalkhambkar, R. G. Inhibition effects of some Schiff's bases on the corrosion of mild steel in hydrochloric acid solution. *Corros. Sci.* **50**, 3356–3362 (2008).

73. Tang, Y., Yang, X., Yang, W., Chen, Y. & Wan, R. Experimental and molecular dynamics studies on corrosion inhibition of mild steel by 2-amino-5-phenyl-1, 3, 4-thiadiazole. *Corros. Sci.* **52**, 242–249 (2010).
74. El Achouri, M. *et al.* Corrosion inhibition of iron in 1 M HCl by some gemini surfactants in the series of alkanediyl- $\alpha$ ,  $\omega$ -bis-(dimethyl tetradecyl ammonium bromide). *Prog. Org. Coat* **43**, 267–273 (2001).
75. Hanza, A. P., Naderi, R., Kowsari, E. & Sayebani, M. Corrosion behavior of mild steel in H<sub>2</sub>SO<sub>4</sub> solution with 1,4-di [1'-methylene-3'-methyl imidazolium bromide]-benzene as an ionic liquid. *Corros. Sci.* **107**, 96–106 (2016).
76. Mertens, S. F., Xhoffer, C., Decooman, B. C. & Temmerman, E. Short-term corrosion of polymer-coated 55% Al-zn- part 1: Behavior of thin polymer films. *Corrosion* **53**, 381–388 (1997).
77. Noor, E. A. & Al-Moubaraki, A. H. Thermodynamic study of metal corrosion and inhibitor adsorption processes in mild steel/1-methyl-4[4'(-X)-styrylpyridinium iodides/hydrochloric acid systems. *Mater. Chem. Phys.* **110**, 145–154 (2008).
78. Al-Mazaideh, G. *et al.* DFT calculations of *Mesembryanthemum nodiflorum* compounds as corrosion inhibitors of aluminum. *Phys. Sci. Int. J.* **12**, 1–7 (2016).
79. Caignan, G. A., Metcalf, S. K. & Holt, E. M. Thiophene substituted dihydropyridines. *J. Chem. Cryst.* **30**, 415–422 (2000).
80. Boumhara, K., Tabyaoui, M., Jama, C. & Bentiss, F. Artemisia Mesatlantica essential oil as green inhibitor for carbon steel corrosion in 1 M HCl solution: Electrochemical and XPS investigations. *J. Ind. Eng. Chem.* **29**, 146–155 (2015).
81. Sastri, V. S., Elboudaini, M., Brown, J. R. & Perumareddi, J. R. Surface analysis of inhibitor films formed in hydrogen sulfide medium. *Corrosion* **52**, 447–452 (1996).
82. ElHamdani, N., Fdil, R., Tourabi, M., Jama, C. & Bentiss, F. Alkaloids extract of *Retama monosperma* (L.) Boiss Seeds used as novel eco-friendly inhibitor for carbon steel corrosion in 1 M HCl solution: Electrochemical and surface studies. *App. Surf. Sci.* **357**, 1294–1305 (2015).
83. Fouda, A. S., Etaiw, S. E. H., Ibrahim, A. M. & El-Hossiany, A. A. Insights into the use of two novel supramolecular compounds as corrosion inhibitors for stainless steel in a chloride environment: Experimental as well as theoretical investigation. *RSC Adv.* **13**, 35305 (2023).
84. Mumit, M. A. *et al.* DFT studies on vibrational and electronic spectra, HOMO–LUMO, MEP, HOMA, NBO and molecular docking analysis of benzyl-3-N-(2, 4, 5-trimethoxyphenylmethylene) hydrazinecarbodithioate. *J. Mol. Struct.* **1220**, 128715 (2020).
85. Ashassi-Sorkhabi, H., Shaabani, B. & Seifzadeh, D. Effect of some pyrimidinic Schiff bases on the corrosion of mild steel in hydrochloric acid solution. *Electrochim. Acta* **50**, 3446–3452 (2005).
86. Shaban, S. M. Studying the effect of newly synthesized cationic surfactant on silver nanoparticles formation and their biological activity. *J. Mol. Liq.* **216**, 137–145 (2016).
87. Negm, N. A. & Morsy, S. M. Corrosion inhibition of triethanolammonium bromide mono- and dibenzoate as cationic inhibitors in an acidic medium. *J. Surf. Det.* **8**, 283–287 (2005).
88. Sastri, V. S. & Perumareddi, J. R. Molecular orbital theoretical studies of some organic corrosion inhibitors. *Corros. Sci.* **53**, 617–622 (1997).
89. Yadav, M., Sarkar, T. K. & Purkait, T. Amino acid compounds as eco-friendly corrosion inhibitor for N80 steel in HCl solution: Electrochemical and theoretical approaches. *J. Mol. Liq.* **212**, 731–738 (2015).
90. Yousif, E. *et al.* Furosemide as an environmental-friendly inhibitor of corrosion of zinc metal in acid medium: Experimental and theoretical studies. *Int. J. Electrochem. Sci.* **102**, 1708–1715 (2015).
91. Kumar, S. H. & Karthikeyan, S. Torsamide and Furosemide as green inhibitors for the corrosion of mild steel in hydrochloric acid medium. *Ind. Eng. Chem. Res.* **52**, 7457–7469 (2013).
92. El-Desoky, A. M., Hytham, A. M. & Alaa, E. A. Electrochemical and analytical study of the corrosion inhibitory behavior of expired pharmaceutical compounds for C-steel corrosion. *Int. J. Electrochem. Sci.* **10**(6), 5112–5129 (2015).
93. Bedair, M. A., Abuelela, A. M., Alshareef, M., Owda, M. & Eliwa, E. M. Ethyl ester/acyl hydrazide-based aromatic sulfonamides: Facile synthesis, structural characterization, electrochemical measurements and theoretical studies as effective corrosion inhibitors for mild steel in 1.0 M HCl. *RSC Adv.* **13**(1), 186–211 (2023).

## Author contributions

S.A.E.M.: suggest the protocol of the paper, write the paper and discuss the results, putting the paper in the final form before submission. A.E.-A.F.: he and S.A.E.M. suggest the protocol of the paper, and participate in the discussion. H.B.: the experimental part is done by him.

## Funding

Open access funding provided by The Science, Technology & Innovation Funding Authority (STDF) in cooperation with The Egyptian Knowledge Bank (EKB).

## Competing interests

The authors declare no competing interests.

## Additional information

**Correspondence** and requests for materials should be addressed to S.A.E.

**Reprints and permissions information** is available at [www.nature.com/reprints](http://www.nature.com/reprints).

**Publisher's note** Springer Nature remains neutral with regard to jurisdictional claims in published maps and institutional affiliations.



**Open Access** This article is licensed under a Creative Commons Attribution 4.0 International License, which permits use, sharing, adaptation, distribution and reproduction in any medium or format, as long as you give appropriate credit to the original author(s) and the source, provide a link to the Creative Commons licence, and indicate if changes were made. The images or other third party material in this article are included in the article's Creative Commons licence, unless indicated otherwise in a credit line to the material. If material is not included in the article's Creative Commons licence and your intended use is not permitted by statutory regulation or exceeds the permitted use, you will need to obtain permission directly from the copyright holder. To view a copy of this licence, visit <http://creativecommons.org/licenses/by/4.0/>.

© The Author(s) 2024